

Impact of Varying Atmospheric Profiles on Extensive Air Shower Observation:

- Fluorescence Light Emission and Energy Reconstruction -

B. Keilhauer^{a,*}, J. Blümer^{a,b}, R. Engel^b, H.O. Klages^b

^a*Universität Karlsruhe, Institut für Experimentelle Kernphysik, Postfach 3640,
76021 Karlsruhe, Germany*

^b*Forschungszentrum Karlsruhe, Institut für Kernphysik, Postfach 3640, 76021
Karlsruhe, Germany*

Abstract

Several experiments measure the fluorescence light produced by extensive air showers in the atmosphere. This light is converted into a longitudinal shower profile from which information on the primary energy and composition is derived. The fluorescence yield as the conversion factor between light profile measured by EAS experiments and physical interpretation of showers has been measured since several decades in laboratory experiments. The results however differ considerably. Therefore, models of the fluorescence emission from several band systems of nitrogen in dependence on wavelength and atmospheric conditions are presented in the article. The model introduced here is compared with measurements and the altitude-dependence of the fluorescence yield is discussed in detail.

PACS: 96.40.Pq

Key words: fluorescence light emission; extensive air shower; atmosphere

1 Introduction

This is the second article of a series of investigations of the importance of atmospheric properties for the reconstruction of extensive air showers (EAS). The first article [1] describes the effect of changing atmospheric density profiles on the longitudinal EAS development. In particular while applying the fluorescence technique, the conversion of atmospheric depth, as used in shower simulations, to geometrical altitude, as reconstructed from the fluorescence

* Corresponding author. *E-mail-Address:* bianca.keilhauer@ik.fzk.de

measurements, and vice versa is very important for the primary mass reconstruction.

This article addresses the fluorescence light emission of EAS which is used for the determination of the total energy of EAS. In several air shower experiments, for example, HiRes [2], the Pierre Auger Observatory [3,4,5], and Telescope Array [6,7], the fluorescence technique is employed for detecting EAS. Measuring the fluorescence light that nitrogen molecules emit after being excited by charged particles traversing the atmosphere, is the most direct method of detecting the longitudinal shower profile. For the event reconstruction procedures of these air shower experiments, the knowledge of the fluorescence yield FY_λ and its dependence on atmospheric conditions are crucial parameters.

The Pierre Auger Observatory is up to now the only existing EAS experiment which applies hybrid detection techniques. The secondary particles of an EAS are measured at ground and simultaneously the fluorescence light of the longitudinal shower development is detected with telescopes. For extracting a cosmic ray spectrum from the data, the events detected with ground detectors are analyzed while the energy calibration is deduced from fluorescence detector events and the correlation of these two types of events is derived from hybrid events [8]. This cosmic ray spectrum and its comparison with spectra published by other experiments (AGASA [9] and HiRes [10] or as a review of experimental results in [11]) reveal that the fluorescence yield might be a crucial parameter for the energy reconstruction of air showers. For the conversion of detected fluorescence light to energy deposited in the atmosphere by EAS and finally to the total energy of the primary particle, not only the entire amount of fluorescence yield in the detected wavelength (λ) region is important but also the spectral distribution. The emitted light suffers *Rayleigh* scattering while traversing the atmosphere towards the telescopes. Since the scattering cross section features a λ^{-4} dependence, the long-wavelength part of the fluorescence spectrum has a higher transmission than the short-wavelength region.

The outline of this paper is as follows. In Section 2, the fluorescence emission in air is discussed and an analytic model (Sec. 2.1) for calculating the fluorescence emission in dependence on wavelength and atmospheric conditions is introduced. Particularly, the band systems of nitrogen contributing mainly to the fluorescence light emission are denoted. A compilation of several parameters from different authors used within the calculations is given in Sec. 2.2. A detailed comparison of measurements with the new model is given in Sec. 3. The aim is to connect the laboratory measurements with the understanding of the processes in the atmosphere, to show possible sources of uncertainty, and to provide an easy way of implementing varying atmospheric conditions. The dependence on these atmospheric conditions is explicitly presented in Sec. 4.

2 Model for Fluorescence Light Emission in Air

The most numerous charged particles in an EAS are electrons and positrons. Their energy deposit in air by ionization and excitation of air molecules is giving rise to fluorescence light emission. In the wavelength region between 300 and 400 nm most of the emitting band systems have been found since the fluorescence light is brightest for these wavelengths. Therefore, all EAS experiments using the fluorescence technique apply UV filters with largest transmittance between roughly 310 and 400 nm. The residual wavelengths are cut for reducing the night sky background.

The major components of the atmosphere are 78.08 *vol%* N₂, 20.95 *vol%* O₂, and 0.93 *vol%* Ar. All three constituent parts influence the emission of fluorescence light, however with strongly differing importance.

Argon can be excited by the reaction $e + Ar \rightarrow Ar^*$, where the excitation cross section is largest for Ar(³P₂) [12]. This process is followed by Ar^{*} + N₂ \rightarrow Ar + N₂^{*}(C³Π_u). The energy is mainly transferred from argon to nitrogen via secondary electrons rather than direct collisions [13]. The excited state C³Π_u is the upper level of the second-positive (2P) system of N₂ which radiates photons mainly in the wavelength region between 300 and 400 nm. The lower state is B³Π_g. This increase of the emission competes however with a higher quenching rate, means non-radiative de-excitation, due to additional collision partners in the form of argon atoms in air. The net effect of argon is expected to be less than 1% contribution to the fluorescence light [14]. However, argon emits also directly fluorescence light at around 310 nm [15]. This transition, A²Σ⁺ – X²Π, has been investigated in argon water-vapor mixtures and the highest intensity has been found for very low argon pressure and 0.06 hPa water vapor. For EAS experiments, this contributions will be of minor importance, too.

The UV-fluorescence light emission from O₂ is negligible [16]. The contribution in the relevant wavelength region stems from O₂⁺ A²Π_u – X²Π_g transmissions. However, already the *Einstein coefficients*² are reduced in average by a factor of about 30 compared to the emissions of the 2P system of N₂ [17]. The emissions of atomic oxygen start at 395 nm and go up to 845 nm [16]. These bands are of no importance for EAS experiments.

The main fluorescence light is emitted by two electronic states of N₂, these are the second-positive (2P) band system, C³Π_u - B³Π_g, and the first-negative (1N) system of N₂⁺, B²Σ_u⁺ - X²Σ_g⁺, see Figs. 1 and 2, respectively. Each band within a system belongs to a transition from a vibrational level of the upper state ν' to a vibrational level of the lower state ν'' . For example, a photography of a glow discharge in a *Geissler* tube filled with air is shown in Fig. 3. The

² radiative transition probabilities

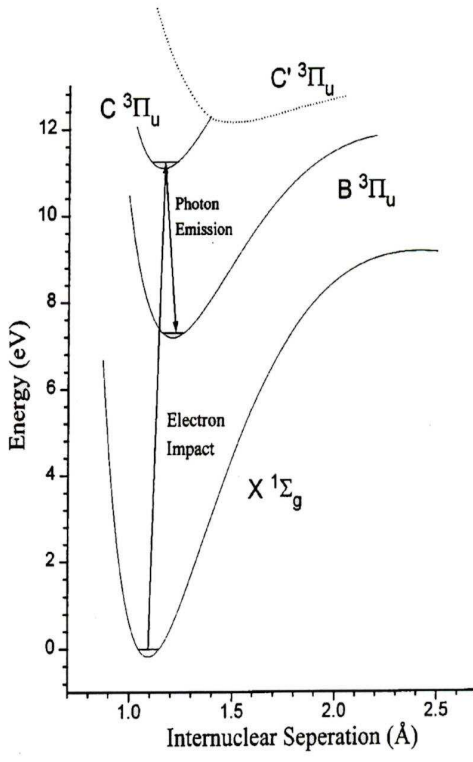


Fig. 1. Electronic energy curves of the nitrogen molecule, showing the relevant energy levels for electron-impact excitation of the second-positive system emissions [18].

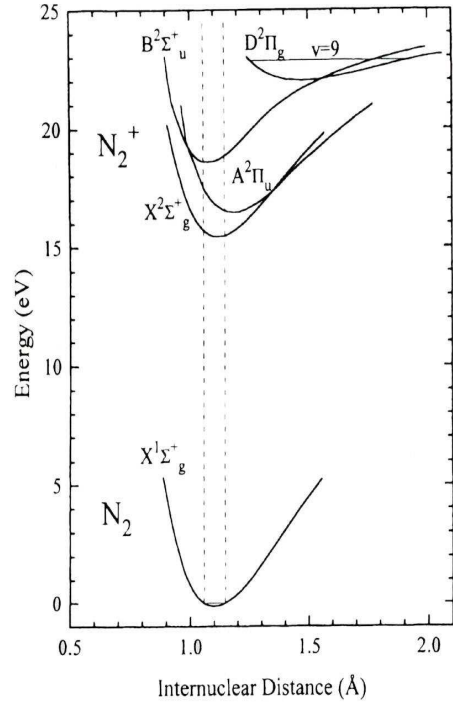


Fig. 2. Energy curves for the ground electronic states of N_2 and N_2^+ and for the first three excited electronic states of N_2^+ [19].

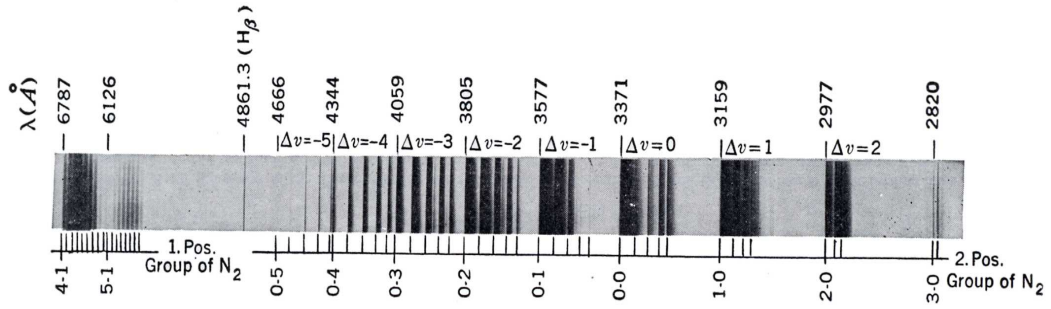


Fig. 3. Photography of a band spectrum of an air-filled Geissler tube. Only the long-wavelength part is shown. [20]

band structure is caused by the rotational levels and consists of a large number of spectral lines which are very close to each other. These lines will not be apportioned in the work, but can be seen exemplarily in Fig. 4. The bands usually have a *band head* at one end where the intensity falls off suddenly. The given wavelength for each band belongs to the position of this band head.

For both, absorption and emission, the *Franck-Condon principle* applies in



Fig. 4. Fine structure of the N_2 band with $\lambda = 380.5$ nm, (0-2) band of the 2P system. The head of the (1-3) band appears at the extreme right. [20]

good approximation. The excitation of N_2 can be discriminated in three processes:

- Direct excitation: The energy deposited in air excites nitrogen molecules proportional to an energy dependent cross section $\sigma_{\nu}(E)$. This process mainly acts on the $\text{N}_2^+ 1\text{N}$ system



- Excitation via secondary electrons: High energy particles in the EAS ionize N_2 producing several lower energy secondary electrons. These e^- are able to excite also the N_2 2P system with a resultant spin change



However, the 2P system can also be excited by cascading from higher levels



- Via *Auger electrons*: Since high energy particles of EAS have about the same probability of interacting with any atomic electron, a certain number of ionizations will release K-electrons which leads to the emission of Auger electrons. These are on their part again able to excite the N_2 molecules.

Generally, it is assumed that the fluorescence light is proportional to the energy deposit of an EAS. The contribution of electrons and positrons to the energy deposit according to the initial kinetic energy distribution in an air shower has been studied elsewhere [21]. Only 10% of the energy deposit stems from particles with energies less than 0.1 MeV, as shown in Fig. 5. Particles with energies between 0.1 and 10 MeV contribute 35%, between 10 and 100 MeV also 35%, and between 100 and 1000 MeV 17%. The remaining 3% originate from particles of energy above 1000 MeV. Several experiments have recently started to measure the proportionality of fluorescence yield to energy deposit. So far none of the results on the energy dependence is absolutely calibrated, thus a direct comparison is difficult. First relative results seem to confirm the expected correlation in different energy regions, see e.g. below 1 keV Arqueros

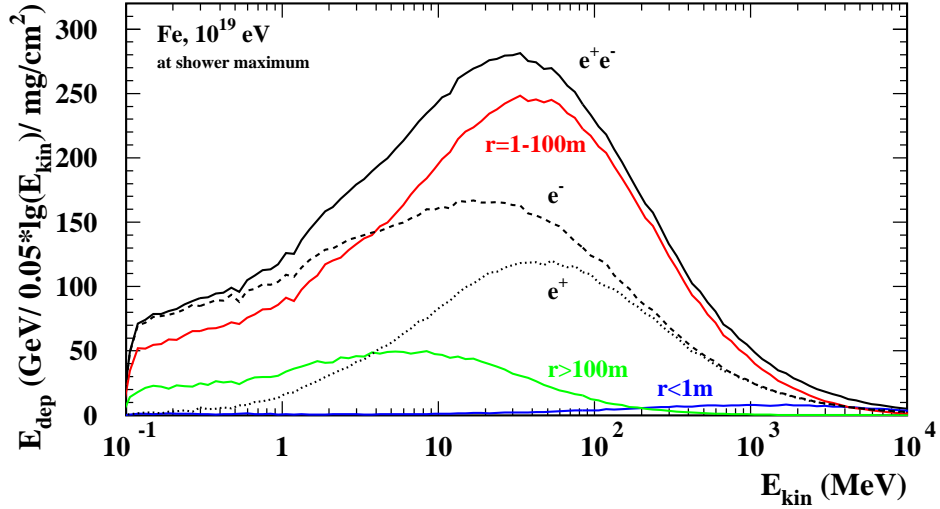


Fig. 5. Contribution to E_{dep} in the next vertical 1 mg/cm^2 as a function of the initial particle energy. Simulations for primary iron, 10^{19} eV , at shower maximum. The sum e^\pm and their individual distributions are shown. Additionally, the total contribution has been divided in three different distance ranges from the shower axis as indicated. The choice of a very thin layer ensures a small relative energy loss of the penetrating particle [21].

et al. [22], at about 1 MeV Nagano et al. [23], between 50 and 420 MeV Bohacova et al. [24], and at 28.5 GeV Belz et al. [25].

In air, however, the optical emission of the prompt radiative return from the upper states of the 2P and 1N system of nitrogen will be affected by some competing processes. The most important process is collisional quenching. Excited nitrogen molecules might collide with other molecules in air before the de-excitation via fluorescence light emission happens. Thus the molecules de-excite via a non-radiative process which leads for the EAS experiments to a smaller photon yield per energy deposit. For the models described in this paper, this effect will be calculated quantitatively using the kinetic gas theory.

Depending on their initial energy, the EAS particles produce secondary electrons with various low energies. These can excite the N_2 but they may suffer an *attachment process*: if, on their way from the production site to the N_2 molecules, the secondary electrons encounter a strong electronegative pollutant (e.g. O_2 , H_2O , CO_2 , H_2 , Xe , CH_4 which are trace gases in the atmosphere), they are attached to this pollutants and cannot excite the N_2 molecules anymore [13]. This process is beyond the scope of this paper.

2.1 Mathematical Description

The existing results of fluorescence yield measurements show quite large differences. Furthermore, the data have to be applied to air shower reconstruction procedures. While secondary particles of EAS traverse from high to low altitudes, they encounter continuously changing atmospheric conditions. Additionally, the atmospheric conditions vary from day to day with the largest contrast between the seasons summer and winter at the sites of all existing air shower experiments. The aim of the calculations shown here is to crosscheck the laboratory measurements with the understanding of the processes in the atmosphere, show possible sources of uncertainties, and provide an easy way of implementing varying atmospheric conditions.

The efficiency of fluorescence light emission can be defined as

$$\frac{\text{rate of de-excitation via radiation}}{\text{total rate of de-excitation}} = \frac{\tau_c}{\tau_0 + \tau_c}, \quad (4)$$

where the rate of de-excitation is proportional to the reciprocal of the life time. The mean life time of the radiative transition to any lower state is τ_0 and to collisional quenching τ_c . The collisional quenching can be described by the kinetic gas theory. The molecules, in the case of air, move with velocities following the Maxwell-Boltzmann-distribution which is strongly correlated with gas temperature. As a good approximation, the collision rate depends on the mean velocity of molecules $\bar{v} = \sqrt{\frac{8kT}{\pi M}}$. The resulting mean life time due to collisional quenching is the ratio of the mean free path, in this case for molecules of one type moving with roughly the same velocity, and the mean velocity:

$$\tau_c = (\sqrt{2} \cdot \rho_n \cdot \sigma_{NN} \cdot \bar{v})^{-1} = \sqrt{(\pi M/kT)} \cdot (4\rho_n \cdot \sigma_{NN})^{-1}, \quad (5)$$

where ρ_n is the particle number density, σ_{NN} the collisional cross section between nitrogen molecules, T the temperature, k the Boltzmann constant, and M the molecular mass. Now the fluorescence efficiency can be defined as

$$\varepsilon_\lambda(p, T) = \frac{\varepsilon_\lambda^0}{1 + (p/p'_{\nu'}(T))} = \frac{n \cdot E_\gamma}{E_{dep}}, \quad (6)$$

with ε_λ^0 being the fluorescence efficiency at wavelength λ without collisional quenching, n denoting the number of photons, E_γ the energy of a single photon with the corresponding wavelength, E_{dep} the deposited energy in the observed medium, and $p/p'_{\nu'} = \tau_{0,\nu'}/\tau_{c,\nu'}$. The pressure p is that of the observed medium (e.g. air), $p'_{\nu'}$ is a reference pressure at which τ_0 is equal to τ_c . $\tau_{0,\nu'}$ and $\tau_{c,\nu'}$ are the mean life times for excitation level ν' . Applying actual atmospheric

conditions, with air presumed to be a two-component gas, the relation between p and $p'_{\nu'}$ can be written as

$$\frac{p}{p'_{\nu'}} = \tau_{0,\nu'} \cdot \left(\frac{1}{\tau_{\text{NN},\nu'}(\sigma_{\text{NN},\nu'})} + \frac{1}{\tau_{\text{NO},\nu'}(\sigma_{\text{NO},\nu'})} \right) \quad (7)$$

$$= \frac{\tau_{0,\nu'} p_{\text{air}} \cdot N_A}{R \cdot T} \cdot \sqrt{\frac{kTN_A}{\pi}} \times \left(4 \cdot \text{vol\%}(N_2) \cdot \sigma_{\text{NN},\nu'} \sqrt{\frac{1}{M_{m,\text{N}}}} \right. \\ \left. + 2 \cdot \text{vol\%}(O_2) \cdot \sigma_{\text{NO},\nu'} \sqrt{2(\frac{1}{M_{m,\text{N}}} + \frac{1}{M_{m,\text{O}}})} \right), \quad (8)$$

with Avogadro's number N_A , the masses per mole for nitrogen $M_{m,\text{N}}$ and oxygen $M_{m,\text{O}}$, the universal gas constant R , and the cross sections for collisional de-excitation for nitrogen-nitrogen $\sigma_{\text{NN},\nu'}$ and nitrogen-oxygen $\sigma_{\text{NO},\nu'}$.

2.2 Input Parameters

These equations imply some parameters which have to be obtained by measurements and/or calculations. Most important is the fluorescence efficiency without collisional quenching ε_{λ}^0 . An early measurement performed by Bunner [14] provides these values for 18 band systems of the 2P and for 1 band system of the 1N state of nitrogen in the wavelength region between 300 and 400 nm. In a more recent publication by Gilmore et al. [17], the Einstein coefficients $A_{\nu'\nu''}$ of the 2P nitrogen state for the transitions from $\nu' = 0 \dots 4$ to $\nu'' = 0 \dots 21$ and the radiative life times $\tau_{0,\nu'}$ for $\nu' = 0 \dots 4$ are given. For the 1N nitrogen state, the Einstein coefficients $A_{\nu'\nu''}$ for the transitions from $\nu' = 0 \dots 10$ to $\nu'' = 0 \dots 21$ and the radiative life times $\tau_{0,\nu'}$ for $\nu' = 0 \dots 10$ are listed. The intensity of a transition could be calculated by $N_{\nu' \rightarrow \nu''} = \tau_{0,\nu'} \cdot A_{\nu'\nu''} \cdot N_{\nu'}^*$, where $N_{\nu'}^*$ is the number of excited states. Since this number is unknown, a relative fluorescence efficiency can be calculated by multiplying the Einstein coefficients with the radiative life times and a *relative apparent excitation cross section* Q_{app} [18]. These Q_{app} values are given in the publication by Fons et al. [18], however only for the 2P band system of nitrogen for $\nu' = 0 \dots 4$. The relative fluorescence efficiency can then be normalized to e.g. the most prominent band of the efficiencies given by Bunner, the 2P(0-0) band system of nitrogen with a wavelength of 337.1 nm. The fluorescence efficiency calculated this way is labeled with $\varepsilon_{\lambda,G.-F.}$. The values used within this paper are listed in Tab. 1. No information is given in Fons et al. for the 1N band system. However, a comparison of the products of the Einstein coefficients and the radiative life times, assuming similar decrease in the relative apparent excitation cross section for the 1N ν' states, indicates measurable contribution for 1N (0-0) = 391.4 nm, 1N (1-0) = 358.2 nm, 1N

Table 1

Constants for the fluorescence efficiency ε_{λ}^0 for nitrogen.

Band ($\nu' - \nu''$)	Wave- length λ (nm)	$\varepsilon_{\lambda, Bunner}^0$ (%)	Gilmore et al. [17]		Fons et al. [18]	$\varepsilon_{\lambda, G.-F.}^0$ (%)
			$A_{\nu' \nu''}$ (1/s)	$\tau_{0, \nu'}$ (s)	Q_{app}	
2P (0-0)	337.1	.082	1.31E7	3.71E-8	1	.082
2P (0-1)	357.7	.0615	8.84E6	3.71E-8	1	.0553
2P (0-2)	380.5	.0213	3.56E6	3.71E-8	1	.0223
2P (1-0)	315.9	.050	1.19E7	3.75E-8	0.7	.0527
2P (1-1)	333.9	.0041	5.87E5	3.75E-8	0.7	.0026
2P (1-2)	353.7	.029	5.54E6	3.75E-8	0.7	.0245
2P (1-3)	375.5	.0271	4.93E6	3.75E-8	0.7	.0218
2P (1-4)	399.8	.016	2.43E6	3.75E-8	0.7	.0108
2P (2-1)	313.6	.029	1.01E7	3.81E-8	0.26	.0169
2P (2-2)	330.9	.002	7.99E5	3.81E-8	0.26	.0013
2P (2-3)	350.0	.004	1.71E6	3.81E-8	0.26	.0029
2P (2-4)	371.0	.010	4.04E6	3.81E-8	0.26	.0068
2P (2-5)	394.3	.0064	3.14E6	3.81E-8	0.26	.0052
2P (3-2)	311.7	.005	5.94E6	3.90E-8	0.081	.0032
2P (3-3)	328.5	.0154	2.85E6	3.90E-8	0.081	.0015
2P (3-4)	346.9	.0063	1.15E5	3.90E-8	0.081	.0001
2P (3-5)	367.2	.0046	2.35E6	3.90E-8	0.081	.0013
2P (3-6)	389.5	.003	3.00E6	3.90E-8	0.081	.0016
2P (4-3)	310.4	-	3.02E6	4.04E-8	0.041	.0008
2P (4-4)	326.8	-	3.71E6	4.04E-8	0.041	.0010
2P (4-5)	344.6	-	1.24E5	4.04E-8	0.041	.0000
2P (4-6)	364.2	-	9.98E5	4.04E-8	0.041	.0003
2P (4-7)	385.8	-	2.33E6	4.04E-8	0.041	.0007
1N (0-0)	391.4	.33	1.14E7	6.23E-8	-	-

$(1-1) = 388.4$ nm, $1N (2-0) = 330.8$ nm, $1N (2-1) = 356.4$ nm, $1N (2-2) = 385.8$ nm, $1N (3-1) = 329.9$ nm, $1N (3-2) = 354.9$ nm, $1N (4-2) = 329.3$ nm, and $1N (4-3) = 353.8$ nm. Since the spectral resolution of the experiments is not of the order of 1 nm, several unidentified contributions from the $1N$ band system might have enlarged the values for the identified $2P$ band systems.

Further parameters in the upper equations are the deactivation constants which are the radiative life time $\tau_{0,\nu'}$ and the collisional cross section between nitrogen and nitrogen molecules $\sigma_{NN,\nu'}$ and between nitrogen and oxygen molecules $\sigma_{NO,\nu'}$. The values for $\tau_{0,\nu'}$ obtained by Gilmore et al. are already listed in Tab. 1. Bunner provides collisional cross sections and radiative life times for the most prominent band systems of nitrogen, see Tab. 2. Recent measurements by Morozov et al. [26] were performed for the $2P \nu' = 0, 1$ band systems, see also Tab. 2. For further calculations presented in this article labeled with *Morozov*, the values from Bunner are partly replaced by the newer data by Morozov et al. where available.

Table 2

Deactivation constants for air in the lower atmosphere.

	Bunner [14]			Morozov et al. [26]		
	σ_{NO} (m ²)	σ_{NN} (m ²)	τ_0 (s)	σ_{NN} (m ²)	σ_{Nvapor} (m ²)	τ_0 (s)
$1N \nu = 0$	13E-19	4.37E-19	6.58E-8	-	-	-
$2P \nu = 0$	2.1E-19	1.0E-20	4.45E-8	1.82E-20	8.53E-19	4.17E-8
$\nu = 1$	5.0E-19 ^a	3.5E-20	4.93E-8	3.77E-20	8.04E-19	4.17E-8
$\nu = 2$	7.0E-19 ^a	8.8E-20	4.45E-8	-	-	-
$\nu = 3$	8.0E-19 ^a	1.2E-19	6.65E-8	-	-	-

^a This value is determined by the given results of [14] and not given in his original publication.

The model based on the above shown calculations in combination with the $\varepsilon_{\lambda, Bunner}^0$ and the deactivation constants from *Morozov* is preferred in this paper. It gains from the completeness of the Bunner data and from the accuracy of the measurements from Morozov et al.

3 Comparison with Measurements

Wavelength-dependent results of fluorescence yield measurements have been provided by three experiments [14,27,28]. Bunner lists several intermediate

values: ε_λ^0 , $\varepsilon_\lambda^{s.l.}(p, T)$ in %, and the fluorescence efficiency $\varepsilon_{E_{dep}}^{s.l.}$ in units of photons/MeV of deposited energy $= \varepsilon_\lambda^{s.l.}(p, T) \cdot (\lambda/hc)$, with λ = wavelength, c = speed of light, h = Planck's constant, at sea level (*s.l.*). The values for $\varepsilon_\lambda^{s.l.}(p, T)$ and $\varepsilon_{E_{dep}}^{s.l.}$ given explicitly in [14] are not reproduced by the calculations shown here, see Table 3. Possible reasons are rounding uncertainties by Bunner or the use of deviating numbers for variables concerning air conditions. Davidson and O'Neil [28] list results for $\varepsilon_\lambda^{s.l.}(p, T)$ for wavelengths above 320 nm. It should be mentioned that the results in [28] are given for $p = 800$ hPa. The increase of the total fluorescence yield between 300 and 400 nm from sea level with $p = 1013$ hPa to approximately 2 km a.s.l. with $p = 800$ hPa amounts to about 2%. Nagano et al. report directly the values for FY_λ at sea level for 0.85 MeV electrons [27], however, only 10 contributing emission bands are listed. For comparing the results of all authors, 0.85 MeV electrons are chosen as exciting particles, so the ionization energy deposit is $dE/dX = 0.1677$ MeV/kg·m⁻² [23]. It is assumed that the fluorescence yield is proportional to the energy deposit as discussed in Sec. 2. Air is taken to be a composition of 78.8 vol% N₂ and 21.1 vol% O₂ [23]. The resulting fluorescence yield can be written as

$$FY_\lambda = \varepsilon_\lambda(p, T) \cdot \frac{\lambda}{hc} \cdot \frac{dE}{dX} \cdot \rho_{air} \left[\frac{\text{photons}}{\text{m}} \right]. \quad (9)$$

A comparison of the obtained FY_λ values at sea level in the US Standard Atmosphere (US-StdA) [29,1] is shown in Table 3 and illustrated in Fig. 6.

The total fluorescence yield reported by Bunner directly in [14] is much lower than the other measurements and calculations. The total value from Davidson and O'Neil is higher by 6.8% for wavelengths above 320 nm as compared to our model for the same wavelength region. The calculations shown here applying $\varepsilon_{\lambda, \text{Bunner}}^0$ reproduce the measured values from Nagano et al. very accurately and the partly varying deactivation constants from Bunner and Morozov et al. do not affect the final result much. However, this holds only for the comparison of the whole wavelength region between 300 and 400 nm. One difficulty in the measurements is the treatment of interference filters which have a bandwidth of about 10 nm [27]. The 10 contributions of Nagano et al. are given after subtracting additional contributions by smaller emissions within one filter region. Thus, for a direct comparison, one has to take into account only the 10 wavelengths reported in [27] and in this case, the calculations with $\varepsilon_{\lambda, \text{Bunner}}^0$ differ by approximately -7%. For a detailed comparison of each individual band system, see Fig. 7.

The measurements from Nagano et al. show two contributions which are considerably larger than all other data sources for those band systems at 315.9 and 394.3 nm. The largest relative difference occurs at the wavelength 328.5 nm where the value measured by Nagano et al. is higher by 512% compared to

Table 3

Fluorescence yield at sea level in the US Standard Atmosphere. Details see text.

Wave-length λ (nm)	$FY_{\lambda}^{s.l.}$ (photons m ⁻¹) measurements from Bunner [14]	Davidson & O'Neil [28]	Nagano et al. [27]	$FY_{\lambda}^{s.l.}$ (photons m ⁻¹) calculations with $\varepsilon_{\lambda, Bunner}^0$, Table 2_{Bunner}	$\varepsilon_{\lambda, Bunner}^0$, Table $2_{Morozov}$	$\varepsilon_{\lambda, G.-F.}^0$, $\sigma_{Nx, Morozov}$, $\tau_{0, Gilmore}$
310.4	- ^a	- ^b	- ^a	-	-	0.001
311.7	0.008	- ^b	- ^a	0.009	0.009	0.010
313.6	0.090	- ^b	- ^a	0.094	0.094	0.064
315.9	0.224	- ^b	0.549	0.240	0.279	0.326
326.8	- ^a	- ^a	- ^a	-	-	0.002
328.5	0.027	0.035	0.180	0.029	0.029	0.005
330.9	0.007	- ^a	- ^a	0.007	0.007	0.005
333.9	0.019	- ^a	- ^a	0.021	0.024	0.017
337.1	0.887	1.173	1.021	1.169	1.108	1.242
344.6	- ^a	- ^a	- ^a	-	-	0.000
346.9	0.012	0.015	- ^a	0.012	0.012	0.000
350.0	0.014	0.013	- ^a	0.014	0.014	0.012
353.7	0.146	0.188	0.130	0.156	0.181	0.170
357.7	0.707	0.889	0.799	0.931	0.882	0.889
364.2	- ^a	- ^a	- ^a	-	-	0.001
367.2	0.009	0.012	- ^a	0.010	0.010	0.005
371.0	0.037	0.047	- ^a	0.038	0.038	0.030
375.5	0.150	0.187	0.238	0.155	0.180	0.160
380.5	0.261	0.328	0.287	0.343	0.325	0.381
385.8	- ^a	- ^a	- ^a	-	-	0.001
389.4	0.006	- ^a	- ^a	0.007	0.007	0.006
391.4	0.281	0.454	0.302	0.315	0.315	-
394.3	0.025	0.032	0.063	0.026	0.026	0.025
399.8	0.090	0.119	0.129	0.097	0.113	0.085

^a This transition has not been measured.^b Only measurements above 320 nm.

continuation Table 3

Wave-length λ (nm)	$FY_{\lambda}^{s.l.}$ (photons/m) measurements from Bunner [14]	Davidson & O'Neil [28]	Nagano et al. [27]	$FY_{\lambda}^{s.l.}$ (photons/m) calculations with $\varepsilon_{\lambda,Bunner}^0$, Table 2 _{Bunner}	$\varepsilon_{\lambda,Bunner}^0$, Table 2 _{Morozov}	$\varepsilon_{\lambda,G.-F.}^0$, $\sigma_{Nx,Morozov}$, $\tau_{0,Gilmore}$
sum of $\lambda = (300-400)$ nm						
	3.001	3.490 ^b	3.698	3.672	3.651	3.427 ^c
sum of all Nagano-wavelengths						
	2.798	3.405 ^b	3.698	3.460	3.437	3.283 ^c
sum of all Nagano-wavelengths above 320 nm						
	2.574	3.405	3.149	3.221	3.159	2.957 ^c
sum of all Nagano-wavelengths above 320 nm and without 391.4 nm						
	2.293	2.951	2.847	2.906	2.884	2.957

^c Without 1N band system.

the model presented here. However, the absolute contribution of this band emission is only of minor importance for the entire wavelength region between 300 and 400 nm. The calculations based on the Einstein coefficients given by Gilmore et al. lead to typically 20% - 30% lower fluorescence yield than the preferred model. Interestingly, the band emission at 328.5 nm which is very bright in the measurements by Nagano et al. is much lower than our model in the calculations using Gilmore et al. combined with Fons et al. data. These uncertainties might be caused by possible contributions from the 1N system, see Fig. 6.

Hirsh et al. [30] have performed measurements for the 1N (0-0) band system of nitrogen. They found a value for the fluorescence efficiency $\varepsilon_{391.4\text{ nm}}^0$ of 0.475% which is considerably higher than the value given by Bunner, see Table 1. Additionally, the collisional cross section of nitrogen with nitrogen and nitrogen with oxygen have been investigated [30]. The values are $\sigma_{NN} = 6.5 \times 10^{-19} \text{ m}^2$ and $\sigma_{NO} = 10.9 \times 10^{-19} \text{ m}^2$. Calculating the fluorescence yield for a 0.85 MeV electron with these parameters, the value at sea level in the US Standard Atmosphere amounts to 0.377 photons/m. A comparison of this number with the entries in Tab. 3 shows that $FY_{391.4\text{ nm}}$ measured by Hirsh et al. is larger than our model by 20%, larger than measurements by Nagano et al. by 25%, and larger than measurements by Bunner even by 34%. Only measurements performed by Davidson and O'Neil resulted in a 17% higher $FY_{391.4\text{ nm}}$ than Hirsh et al.

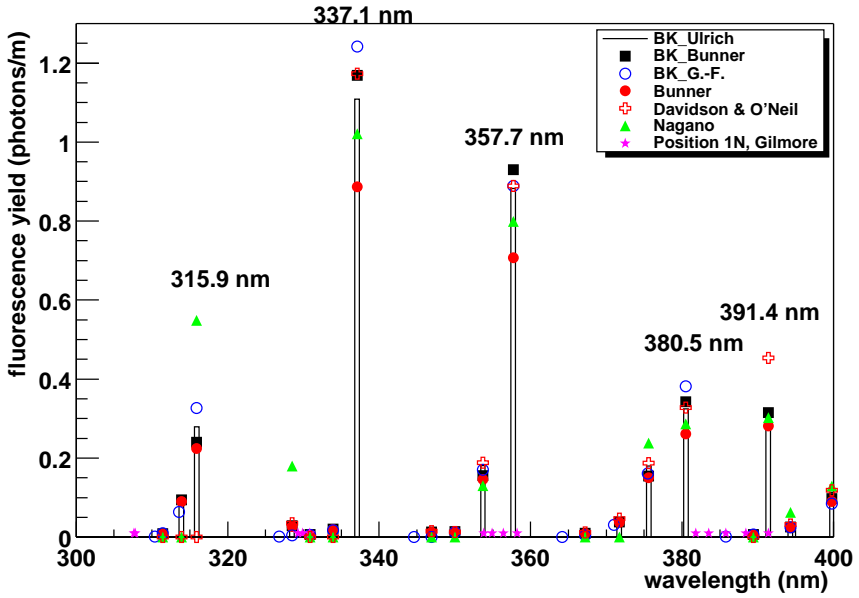


Fig. 6. Fluorescence yield spectra of several calculations and measurements. The bars indicate the preferred model presented in this article. All calculations are labelled with “BK_name”, where *name* indicates the authors of the input parameters. Pink stars indicate the positions of possible contributions of the 1N system beyond the 1N (0-0) transition.

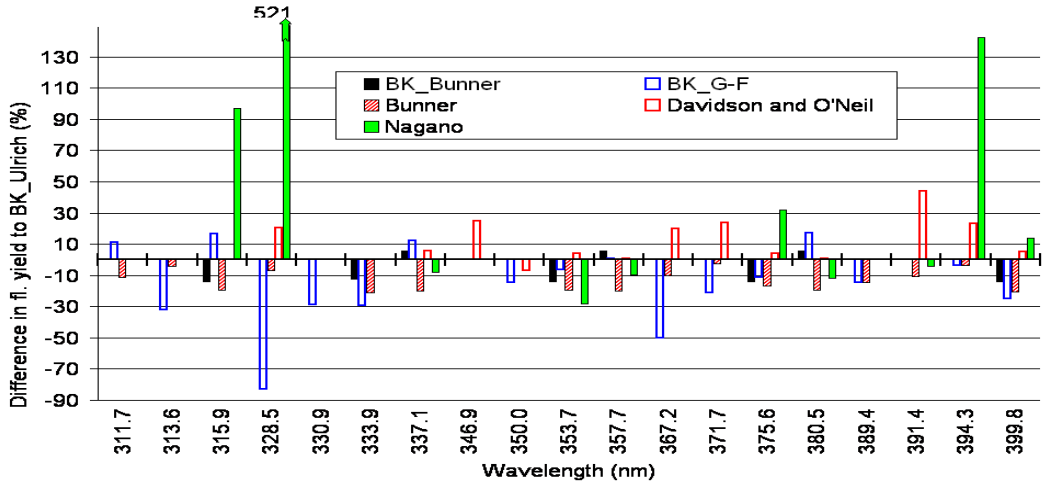


Fig. 7. Relative comparison of 19 band systems of the model introduced in this article with measurements and calculations. The absolute fluorescence yield of these contributions can be seen in Fig. 6 with the same marking.

Concluding, it can be stated that the calculations shown here provide a reasonable way of describing fluorescence emission in air while allowing for varying atmospheric conditions. This procedure can easily be implemented into air shower reconstruction programs. The overall agreement in the wavelength region between 300 and 400 nm with some measurements is already satisfy-

ing. However detailed, spectrally resolved considerations reveal uncertainties in measurements and the understanding of the processes in air. Further investigations are necessary, because emissions at different wavelengths will be scattered with different Rayleigh scattering cross sections. Also the dependence on altitude is different for the emission bands. Thus, for reconstructing the fluorescence emission of an EAS in the atmosphere from the measured photons, all these processes must be understood. It must be stressed that for the EAS experiments the uncertainties in fluorescence yield are directly converted into uncertainties in the primary energy of cosmic rays.

It should also be mentioned that further fluorescence yield measurements can be found in literature without spectral resolution. Kakimoto et al. provide a formula for calculating the fluorescence yield between 300 and 400 nm, which gives at sea level $3.275 \frac{\text{photons}}{\text{m}}$ [31]. This value is smaller by 10.3 % compared to our model. The HiRes Collaboration uses a value of about $5 \frac{\text{photons}}{\text{m}}$ per charged particle in an air shower [32]. For these charged particles, an average energy deposit of $0.22 \text{ MeV/kg m}^{-2}$ is assumed [14], which leads to a corresponding fluorescence yield at s.l. of $3.811 \frac{\text{photons}}{\text{m}}$ for a 0.85 MeV electron. Assuming that the HiRes value refers to 5 km a.s.l., one would obtain at s.l. $3.6 - 3.7 \frac{\text{photons}}{\text{m}}$.

4 Dependence on Atmospheric Conditions

4.1 Altitude Dependence

Firstly, the altitude dependence of the fluorescence efficiency $\varepsilon_{E_{dep}}$ in units of photons/MeV of deposited energy, as described in Section 3, will be shown. Equations (7) and (8) comprise the altitude dependent variables p and T . Combined with the deactivation constants, Tab. 2, a different altitude dependence for the 1N (391.4 nm) and 2P system (all other wavelengths) is expected, which is visualized in Fig. 8. Within the 2P system of nitrogen, there are no differences in the altitude dependence for all emission bands belonging to the same excited state ν' (e.g. 337.1 nm and 357.7 nm) and only small variations are between bands of different ν' states (compare e.g. 315.9 nm from $\nu' = 1$ and 337.1 nm from $\nu' = 0$). With increasing altitude, the efficiency becomes larger due to lower rates of collisional quenching. This increase is largest for the 391.4 nm band. At sea level its contribution to the total spectrum amounts to 8.6%, at 20 km a.s.l. it is already 10.7%, and at 30 km a.s.l. 16.8%. However, regarding EAS, the rate of emitted photons per meter traversed matter of the EAS is the observed variable which is the fluorescence yield FY_λ , eq. (9). Via the altitude-dependent air density ρ_{air} , the number of excitable nitro-

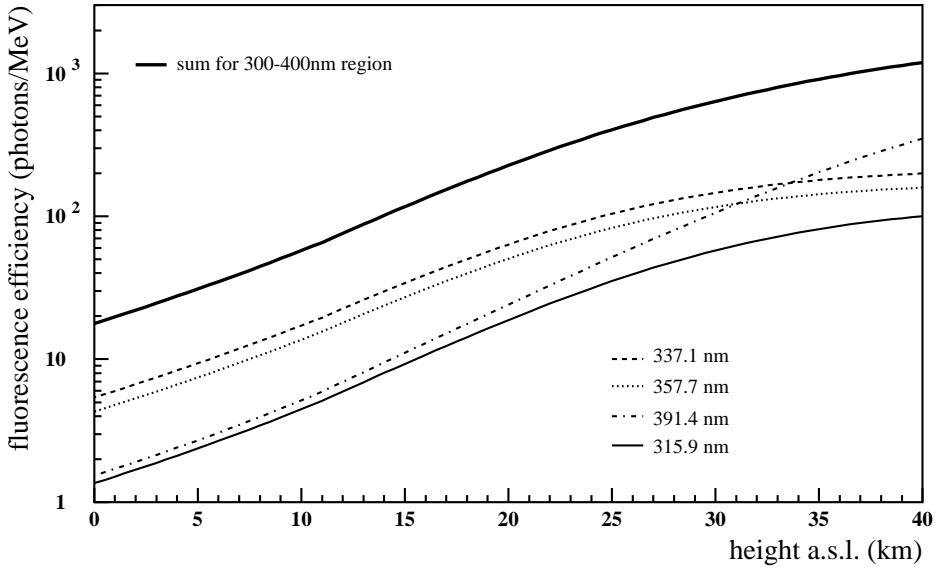


Fig. 8. Fluorescence efficiency profiles for different wavelengths in the US-StdA.

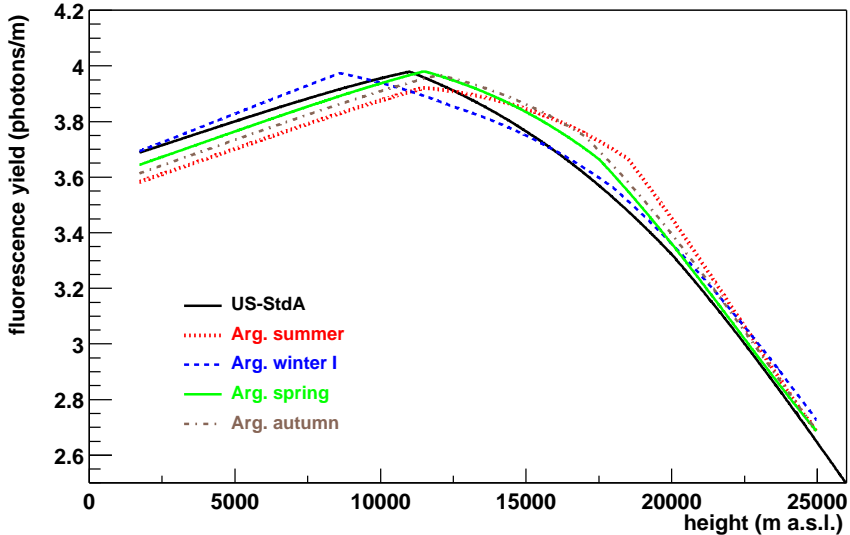


Fig. 9. Fluorescence yield profiles for a 0.85 MeV electron with vertical incidence in the US Standard atmosphere and measured Argentine atmospheres as given in [1]. The given yield is a sum of all emitted photons between 300 and 400 nm calculated as described in Sec. 3 with $\varepsilon_{\lambda, \text{Bunner}}^0$ and Table 2_{Morozov}.

gen molecules and quenching partners are ascertained. For simplicity, FY_λ vs. altitude is shown in Fig. 9 for a 0.85 MeV electron. The most relevant altitude range for EAS is between ground and about 13 km a.s.l. For EAS with energies of about 10^{19} eV, the shower reaches its maximum between 2 and 8 km a.s.l. depending on the type of the primary particle and the inclination angle of the EAS. E.g. for the Auger experiment, the field of view of a telescope

covers an altitude range between 0.7 km and 12.5 km a.s.l. at a distance of 20 km. The fluorescence yield plotted in Fig. 9 is a sum of all emitted photons between 300 and 400 nm calculated as described in Sec. 3 with $\varepsilon_{\lambda, \text{Bunner}}^0$ and Table 2_{Morozov}. Additionally to the altitude dependence, also the seasonal dependence for actual atmospheres as obtained at the southern site of the Pierre Auger Observatory [1] can be seen in Fig. 9. From ground level to altitudes around 10 km, the fluorescence yield increases slowly. Above 10 km, the yield decreases disclosing the sensitivity to temperature and pressure variations. During winter I, the lower temperatures compared to the other atmospheric models below 9 km a.s.l. induce a higher fluorescence yield. Up to 17 km, the temperatures are comparatively warm leading to a reduced fluorescence yield. During spring, summer, and autumn, the temperatures are higher than in the US-StdA, therefore the fluorescence yield is decreased mostly in summer. Above 15 km a.s.l., the very low temperatures during summer result in a very high emission. The differences of FY_{λ} for the Argentine seasons compared to the US-StdA are well below $\pm 5\%$. At *Auger level*, 1.4 km a.s.l., the increase in fluorescence yield during winter I is negligible, however the decrease in summer amounts to 2.9%. At ≈ 8.5 km, the differences of summer and winter I to the US-StdA are in the same size but with opposite signs. In winter I, FY_{λ} is 1.5% higher than in the US-StdA, and in summer 2.2% lower. More than +4% difference from Argentine summer to the US-StdA emerges above 16.5 km a.s.l. Similar seasonal variations in FY_{λ} are also valid for other EAS experiments since similar atmospheric conditions have been found at different places [1,33].

The calculated altitude dependence can be compared with parameterizations given by authors from experiments on the fluorescence emission. They deduce parameterizations of functional forms based on the same equations as introduced in Sec. 2.1 [27,31]:

$$FY_{\lambda}^{[27]} = \frac{dE}{dX} \cdot \left(\frac{A_{\lambda}\rho}{1 + \rho B_{\lambda}\sqrt{T}} \right), \quad (10)$$

$$FY_{300-400 \text{ nm}}^{[31]} = \frac{dE}{dX} \cdot \rho \left(\frac{A_1}{1 + \rho B_1\sqrt{T}} + \frac{A_2}{1 + \rho B_2\sqrt{T}} \right). \quad (11)$$

While Nagano et al. [27] list A and B parameters for each of their 10 wavelengths between 300 and 400 nm, Kakimoto et al. [31] just provide one set of parameters $A_{1,2}$ and $B_{1,2}$ for the total fluorescence yield between 300 and 400 nm. Both approaches predict similar height dependences, see Fig. 10. To work out the difference due to the altitude dependence, the profiles can be shifted so that all curves start with the same value at sea level. Then the parameterization by Nagano et al. agrees very well with the model introduced in this paper. Up to 14 km, the discrepancy is below 1%, increasing up to 2.9% at 20 km a.s.l. The simplified parameterization given by Kakimoto et

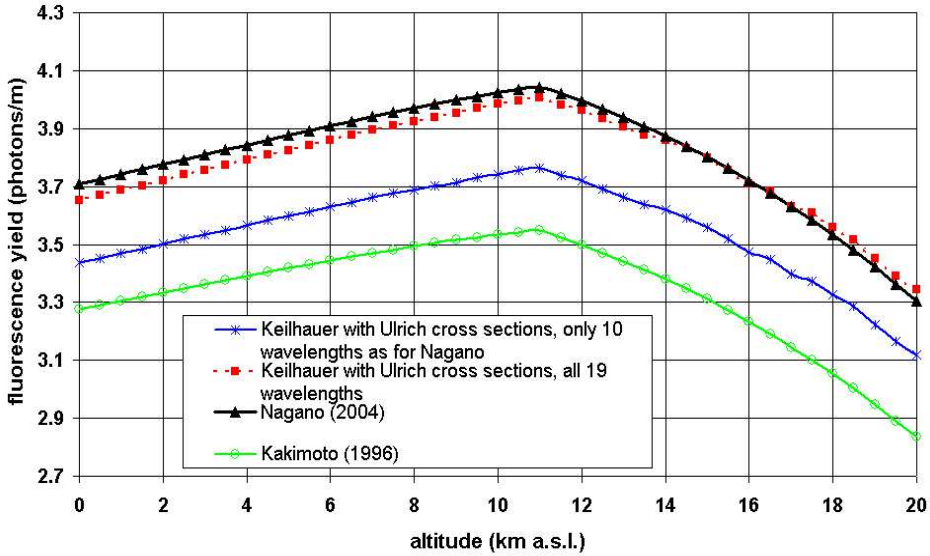


Fig. 10. Fluorescence yield profiles for a 0.85 MeV electron with vertical incidence in the US-StdA. Comparison of the altitude dependence calculated by the described method with two further parameterizations.

al. disagrees already above 6.5 km by more than 1% to the calculations shown here. The difference increases up to 4% at 20 km a.s.l.

4.2 Humidity Dependence

All calculations and measurements shown above are based on dry air conditions. However in actual atmospheric conditions, there is sometimes a considerable content of water vapor. Thus, the effect of quenching due to water vapor has to be investigated. A fluorescence emission by water vapor is not expected.

Our first calculations are based on eq. (8) in which an additional term counts for the collisions between nitrogen and water vapor molecules. The experimental determination of collisional cross sections between nitrogen and water vapor which is needed in that equation is very difficult. Two experiments have begun recently to investigate the effect of water vapor [26,34].

The effect of quenching due to water vapor has been studied in our model for the 337.1 nm emission band. Applying the constants from Tab. 2 by Morozov et al. and assuming 100% relative humidity, the emission at sea level is reduced by approximately 20%, at 4 km a.s.l. by roughly 5%, and at 8 km a.s.l. just by 0.3%. Since fluorescence telescopes typically operate only during “good weather” periods, this decrease in fluorescence yield marks an upper limit.

For realistic atmospheric conditions, an effect of about 5 to 10% near ground and 1 - 3% at 4 km a.s.l. can be expected.

5 Summary and Conclusion

EAS experiments applying the fluorescence technique measure the light emission in air induced by charged particles, mainly electrons and positrons. The detected light track is converted into a longitudinal shower profile and finally to the total energy of the primary particle of the EAS. Therefore, the fluorescence light yield has to be known precisely including spectral resolution and dependent of atmospheric conditions.

The results on fluorescence yield which can be found in literature differ considerably. Most important are the fluorescence efficiency of the contributing band systems of nitrogen, but also the radiative life times and the collisional cross sections of nitrogen with nitrogen and nitrogen with oxygen have to be known. Up to now, a thorough understanding of the energy-dependent excitation processes of the different nitrogen states is missing. First studies can be found in Blanco and Arqueros [35].

In this article, an atmosphere-dependent model of the fluorescence light emission in air has been presented. The different contributions of the 2P and 1N band system of nitrogen have been calculated in detail. The calculations are based on several parameters and have been compared with fluorescence yield measurements performed by several authors. The calculations reproduce some results of measurements well, while other data are off by more than 10% regarding the total yield between 300 and 400 nm. The differences for individual emission bands are much larger.

The variation of the fluorescence yield with changing atmospheric conditions have only been studied by a few authors. Generally, it is assumed that the main reduction of light emission is due to collisional quenching. The calculations of altitude-dependent profiles of FY_λ presented here agree within 4% with parameterizations of measurements.

Using the model preferred in the article, a prediction of the influence of water vapor can be made. Altitudes are chosen which are most important for air shower observation. For realistic atmospheric conditions, an effect of about 5 to 10% near ground and less than 3% at altitudes around 4 km a.s.l. can be expected. Only lately experimental studies of quenching rate of water vapor have begun.

Acknowledgment

One of the authors (BK) is supported by the German Research Foundation (DFG) under contract No. KE 1151/1-1.

References

- [1] B. Keilhauer, J. Blümmer, R. Engel, H. O. Klages, M. Risse, *Astropart. Phys.* **22**, 249, (2004)
- [2] C. C. Jui et al. (HiRes Collab.), in *Invited Rapporteur and Highlight Papers, Proc. 26th Int. Cos. Ray Conf.* (Salt Lake City), 370, (2000)
- [3] A. Etchegoyen et al., FERMILAB-PUB-96-024, <http://www.auger.org/admin/DesignReport/>, (1996)
- [4] J. Blümmer (Pierre Auger Collab.), *J. Phys.* **G29**, 867, (2003)
- [5] J. Abraham el al. (Pierre Auger Collab.), *Nucl. Instr. and Meth. in Phys. Res.* **A523**, 50, (2004)
- [6] M. Fukushima et al. (TA Collab.), <http://www-ta.icrr.u-tokyo.ac.jp/TA>, (2000)
- [7] M. Fukushima, *Prog. Theor. Phys. Suppl.* **151**, 206, (2003)
- [8] P. Sommers et al. (Pierre Auger Collab.), *Proc. 29th Int. Cos. Ray Conf.*, Pune, India, (2005)
- [9] AGASA Collaboration, <http://www-akeno.icrr.u-tokyo.ac.jp/AGASA/ressults.html>, (2004)
- [10] R. U. Abbasi et al. (HiRes Collab.), *Phys. Rev. Lett.* **92**, 151101, (2004)
- [11] R. Engel, H. Klages, *C. R. Phys.* **5**, 505, (2004)
- [12] W. R. Bennett, Jr. and J. Flint, *Phys. Rev.* **A18**, 2527, (1978)
- [13] A. E. Grün and E. Schopper, *Z. Naturforschg.* **9a**, 134, (1954)
- [14] A. N. Bunner, *Cosmic Ray Detection by Atmospheric Fluorescence*, PhD thesis, Cornell University, Ithaca, NY, USA, (1967)
- [15] A. Morozov, R. Krücken, T. Ottenthal, J. Wieser, A. Ulrich, *Appl. Phys. Lett.* **86**, 011502, (2005)
- [16] R. W. Nicholls, E. M. Reeves, D. A. Bromley, *Proc. Phys. Soc.* **74**, 87, (1959)
- [17] F. R. Gilmore, R. R. Laher, P. J. Espy, *J. Phys. Chem. Ref. Data* **21**, 1005, (1992)

- [18] J. T. Fons, R. S. Schappe, C. C. Lin, Phys. Rev. **A53**, 2239, (1996)
- [19] J. T. Fons, J. S. Allen, R. S. Schappe, C. C. Lin, Phys. Rev. **A49**, 927, (1994)
- [20] G. Herzberg, Molecular Spectra and Molecular Structure: I. Spectra of Diatomic Molecules, D. van Nostrand Company, Inc., New York, (1950)
- [21] M. Risse and D. Heck, Astropart. Phys. **20**, 661, (2004)
- [22] F. Arqueros, F. Blanco, M. Ortiz, Proc. 29th Int. Cos. Ray Conf., Pune, India, (2005)
- [23] M. Nagano, K. Kobayakawa, N. Sakaki, K. Ando, Astropart. Phys. **20**, 293, (2003)
- [24] M. Bohacova et al., Proc. 29th Int. Cos. Ray Conf., Pune, India, (2005)
- [25] J. W. Belz et al. (FLASH Collab.), astro-ph/0506741, (2005)
- [26] A. Morozov, R. Krücke, J. Wieser, A. Ulrich, Eur. Phys. J. **D33**, 207, (2005)
- [27] M. Nagano, K. Kobayakawa, N. Sakaki, K. Ando, Astropart. Phys. **22**, 235, (2004)
- [28] G. Davidson and R. O'Neil, J. Chem. Phys. **41**, No. 12, 3946, (1964)
- [29] National Aeronautics and Space Administration (NASA), U.S. Standard Atmosphere 1976, NASA-TM-X-74335, (1976)
- [30] M. N. Hirsh, E. Poss, P. N. Eisner, Phys. Rev. **A1**, 1615, (1970)
- [31] F. Kakimoto et al., Nucl. Instr. and Meth. in Phys. Res. **A372**, 527, (1996)
- [32] R. U. Abbasi et al. (HiRes Collab.), Astrophys. J. **622**, 901, (2005)
- [33] B. Wilczynska et al., Proc. 29th Int. Cos. Ray Conf., Pune, India, (2005)
- [34] N. Sakaki, K. Kobayakawa, M. Nagano, Y. Watanabe, Proc. 29th Int. Cos. Ray Conf., Pune, India, (2005)
- [35] F. Blanco and F. Arqueros, Phys. Lett. **A345**, 355, (2005)